View Online
Dynamic Article Links

Dalton Transactions

Cite this: DOI: 10.1039/c1dt10740b

www.rsc.org/dalton

PAPER

Sorption Speciation of Nickel(II) onto Ca-Montmorillonite: Batch, EXAFS Techniques and Modeling†

XiaoLi Tan,*[a] Jun Hu,[a] Gilles Montavon[b] and XiangKe Wang*[a]

Received 22nd April 2011, Accepted 3rd August 2011
DOI: 10.1039/c1dt10740b

The sorption speciation of Ni(II) on Ca-montmorillonite was evaluated using a combination of batch experiments, extended X-ray absorption fine structure (EXAFS) spectroscopy and modeling. The pH and temperature at the aqueous-montmorillonite interface affects both the extent of Ni(II) sorption as well as the local atomic structure of the adsorbed Ni(II) ions. At 0.001 mol L^{-1} $Ca(NO_3)_2$ and low pH, the study reveals that the majority of Ni(II) is adsorbed in the interlayers of Ca-montmorillonite coordinated by six water molecules in an octahedron as an outer-sphere complex. At higher pH, inner-sphere surface complexes are formed. The Ni–Si/Al distances ($R_{Ni–Al}$ = 3.00 Å, $R_{Ni–Si1}$ = 3.10 Å and $R_{Ni–Si2}$ = 3.26 Å) determined by EXAFS confirm the formation of mononuclear complexes located at the edges of Ca-montmorillonite platelets at pH 7.5 and 8.5. At pH 10.0, the Ni–Ni/Si distances ($R_{Ni–Ni}$ = 3.07 Å and $R_{Ni–Si}$ = 3.26 Å) indicates the formation of Ni-phyllosilicate precipitates. A rise in temperature promotes inner-sphere complexation, which in turn leads to an increase in Ni(II) sorption on Ca-montmorillonite. Sorption edges are fitted excellently by surface complexation model (SCM) with the aid of surface species determined from EXAFS spectroscopy.

1. Introduction

Availability of Ni(II) for bio-uptake and transport in the environment is controlled by sorption processes and speciation of Ni(II). The final form of metal sorption products influences the mobility, bioavailability, and ultimately toxicity in the environment.[1,2] Thus, it is critical to understand Ni(II) sorption speciation in soils.[3–8] However, accurately determining Ni(II) speciation in whole soils is challenging because soils are heterogeneous with respect to mineralogy and composition. This difficulty can be overcome by studying more controlled systems in which major interactions between Ni(II) and specific soil constituents can be isolated. Montmorillonite is present in most soils and aquatic systems, which has been characterized in detail.[8] Montmorillonite presents several types of sorption sites (such as exchange sites, amphoteric edge sites). Ni(II) sorption mechanisms on this mineral are expected to be complex (Fig. 1). The determination of Ni(II) species on montmorillonite allows one to clearly identify the adsorbed Ni(II) species on clay minerals, and to evaluate the interaction of Ni(II) on soils. Understanding metal speciation and sorption complexes can also help to select appropriate management and remediation methods for contaminated environments.

Sorption of Ni(II) on clay minerals has been extensively studied by sorption experiments.[3–12] Many mechanisms have been postulated for Ni(II) sorption, including ion exchange, surface complexation (inner-sphere and outer-sphere), precipitation/coprecipitation, and diffusion into particle micropores.[3–12] However, these approaches did not yield any direct structural information on the adsorbed ions. Recently, extended X-ray absorption fine structure (EXAFS) studies have been a powerful tool for the investigation of Ni(II) speciation on mineral surfaces at atomic level over short time scales at pH levels undersaturated with respect to pure metal hydroxide solubility, and at metal surface coverage below theoretical monolayer coverage.[13–17] Utilizing this method, Scheidegger *et al.*[14] observed the presence of a mixed Ni–Al hydroxide phase at low surface loading and at reaction conditions undersaturated with respect to the formation of $Ni(OH)_2$(s). Dähn *et al.*[17] demonstrated that the uptake of Ni(II) on montmorillonite resulted in the neoformation of a phyllosilicate. They also found that the reaction time may determine the structure of the adsorbed Ni. Often the sorption speciation of metal ions is contingent upon the existent physical and chemical conditions of the system, including solution pH and temperature fluctuation, which can affect the fate and transport of heavy metals in the environment. However, few works were carried out to give structural information of the adsorbed Ni complexes under variable conditions.

Surface complexation modeling (SCM) has successfully described the sorption of metal ions onto adsorbents. However, the

[a]*Key Laboratory of Novel Thin Film Solar Cells, Institute of Plasma Physics, Chinese Academy of Sciences, P.O. Box 1126, Hefei, 230031, P.R. China. E-mail: tanxl@ipp.ac.cn, xkwang@ipp.ac.cn; Fax: +86-551-5591310; Tel: +86-551-5592788*
[b]*Laboratory SUBATECH, Groupe de Radiochimie, UMR Ecole des Mines/CNRS/Université, 4 rue A. Kastler, BP 20722, 44307 Nantes cedex 03, France*

† Electronic supplementary information (ESI) available. See DOI: 10.1039/c1dt10740b

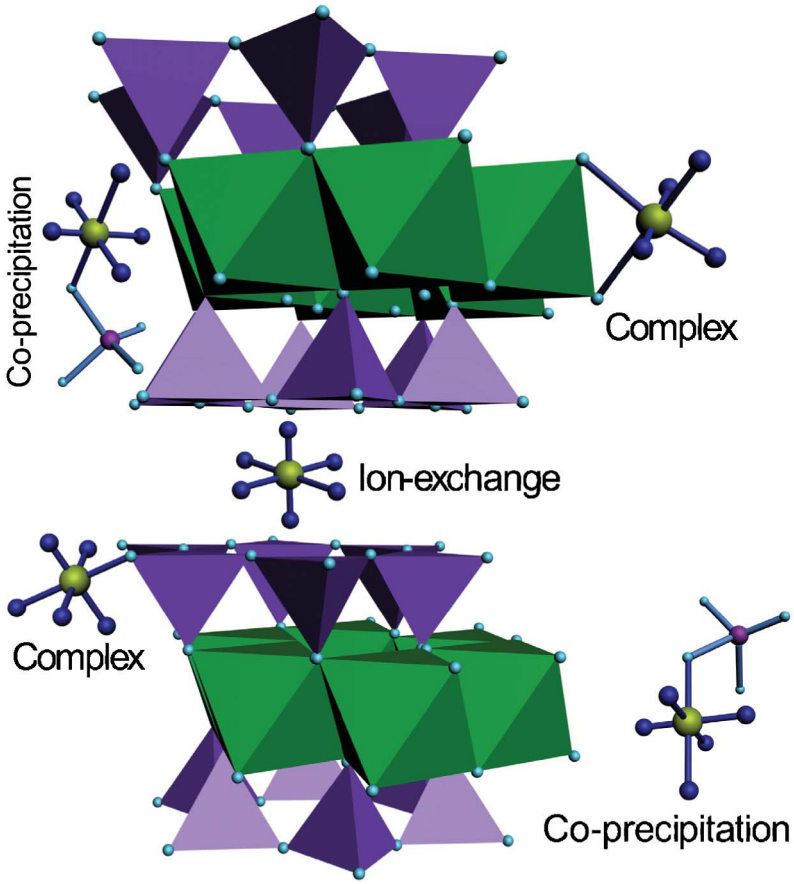

Fig. 1 Illustration of sorption sites for Ni on Ca-montmorillonite.

species are usually determined in the absence of spectroscopic data that may provide more detailed structural information on surface complexes formed.[10–12] To make the sorption mechanisms onto montmorillonite system more reliable, SCM simulation based on spectroscopic data is important. However, to date, only a few reports involve the combination of SCM with spectroscopic investigation, although this may offer a realistic surface complex as far as we know.[18]

In this paper, Ni(II) sorption onto montmorillonite utilizing EXAFS spectroscopy (allowing one to investigate the sorption mechanisms at molecular scale and thus to identify the transition between cation exchange and inner-sphere binding to edge sites at different pH and temperature) was investigated. More importantly, based on the EXAFS data, the SCM simulation of the Ni(II) sorption onto montmorillonite was performed.

2. Experimental Details

2.1 Materials

All solutions were prepared with Milli-Q water. Commercially available Ca-montmorillonite (purity 97%, Zhejiang Sanding Group Co. Ltd., China) was used. The sample of Ca-montmorillonite was rinsed with $Ca(NO_3)_2$ solution and filtration. Then the sample was washed with methanol and dried at 80 °C and used in the experiments. The N_2-BET surface area of Ca-montmorillonite is 64.4 m^2 g^{-1}. The cation exchange capacity (CEC) is 110 mmol/100 g by using the ammonium acetate method,[19] and the point of zero charge (pH_{pzc} ~ 5) is determined by using potentiometric titration method (Fig. SI-1 and Table SI-1†). All chemicals used in the experiments were purchased in analytical purity. Milli-Q water was used in the experiments.

2.2 Sorption Experiments

All the experiments were carried out using batch technique. The Ca-montmorillonite suspension, $Ca(NO_3)_2$, $Ni(NO_3)_2$ stock solution, HNO_3 or buffer were added in the polyethylene test tubes to achieve the desired background electrolyte concentrations and pH of the aqueous solutions. The pH values were adjusted using negligible amounts of HNO_3 (0.1 mol L^{-1} or 0.01 mol L^{-1}) or buffer (4 mmol L^{-1} Tris(hydroxymethyl aminomethane)). The pH values were determined using pH meters by temperature compensation to eliminate the error of the measurements. The test tubes were shaken for 2 weeks and then centrifuged at 9000 rpm for 40 min to separate the solid from liquid phases. The amount of Ni^{2+} adsorbed on Ca-montmorillonite was calculated from the difference between the initial concentration and the equilibrium one. It is necessary to note that the solid-liquid separation by filter for the removal of colloid was not carried out to evaluate the effect of colloid on the sorption of Ni(II) to Ca-montmorillonite. The colloid is important to influence the physicochemical behavior of metal ions. Ni-63 (99.99% purity) was used as radiotracer in the experiments. The carrier free

Ni-63 was dissolved in HNO_3 to achieve radioactive $Ni(NO_3)_2$ solution, which was the same as $Ni(NO_3)_2$ stock solution used in the experiments. The concentration of Ni-63 was analyzed by liquid scintillation counting using a Packard 3100 TR/AB Liquid Scintillation analyzer (PerkinElmer). The scintillation cocktail was ULTIMA GOLD AB (Packard). The separated liquid phases were also analyzed for Si and Al concentrations by optical emission spectroscopy (ICP-OES). The amount of Ni(II) adsorbed on Ca-montmorillonite was calculated from the difference between the initial concentration and the equilibrium one.

The removal of Ni(II) by Ca-montmorillonite was calculated by the following equation:

$$\text{Sorption}\% = \frac{C_0 - C_e}{C_0} \times 100\% \quad (1)$$

where C_0 is the initial concentration of Ni(II), and C_e is the equilibrium one in supernatant after centrifugation.

The amount of metal ions adsorbed on per weight unit of solid after equilibrium (C_s) (mol g^{-1}) is calculated by the following equation:

$$C_s = (C_0 - C_e) \times \frac{V}{m} \quad (2)$$

The distribution coefficient (K_d) was calculated from the initial concentration of Ni(II) in suspension (C_0) and the final concentration of Ni(II) in supernatant (C_e) according to the following equation:

$$K_d = \frac{(C_0 - C_e)}{C_e} \times \frac{V}{m} \quad (3)$$

where V is the volume of the suspension and m is the mass of Ca-montmorillonite.

Detailed sample preparation for EXAFS analysis is shown in the Supporting Information (SI).†

2.3 EXAFS Data Collection and Analysis

Nickel K-edge X-ray absorption spectra at 8333 eV were recorded at room temperature at the national synchrotron radiation laboratory (NSRL, USTC, China) in fluorescence (for Ni^{2+}(aq), Ni/montmorillonite samples) and in transmission (for β-$Ni(OH)_2$) modes. The electron beam energy was 0.8 GeV and the mean stored current was 100 mA. A superconductor wiggler with a maximum magnetic field B_0 of 6 T inserted in the straight section of the storage ring was used. The energy of X-ray was detuned by using a fixed-exit double-crystal Si (111) monochromator. Ionization chambers with N_2 atmosphere were used to collect the Ni K-edge spectra in transmission mode at room temperature. A multi-element pixel high purity Ge solid-state detector (Canberra) was used to collect the fluorescence signal. IFEFFIT and their graphical interfaces ATHENA and ARTEMIS were used for background subtraction and fitting.[20] The input parameter to ATHENA that determines the maximum frequency of the background, R_{bkg}, was set to 1.1 Å.[21] The data range used for Fourier transforming the EXAFS $x(k)$ data was 3.2–12 $Å^{-1}$ with a Kaizer–Bessel window function and a dk value of 0.5 $Å^{-1}$. The amplitude reduction factor S_0^2 was set to 0.85. The theoretical scattering phases and amplitudes used in data analysis were calculated with the scattering code FEFF7[22] using the crystal structure of Ni(II)(aq), β-$Ni(OH)_2$ and Ni-Talc.[23] Errors given were estimated on the basis of the fitting results. The R values were accurate to ± 0.02 Å, and the N values were accurate to ± 20% for the first shell and ± 40% for the second shell.

3. Results and Discussion

3.1 Effect of Solution pH and Temperature on the Ni^{2+} Ion Sorption to Ca-montmorillonite

The sorption of Ni(II) on Ca-montmorillonite as a function of pH was measured in the presence of 0.001 mol L^{-1} $Ca(NO_3)_2$. The variations of Si and Al concentrations in solution during the experiment were also monitored. The concentration of Si amounted to 315 μM and up to 394 μM at different pH. The Al concentration in solution was too low (4 μM) to produce reliable ICP-OES measurements. The Ni sorption results (Fig. 2(A)–(C)) were consistent with previous research which distinguished divalent metal ion sorption on edge and interlayer sites based on the background electrolyte concentration and pH dependence of sorption. The effect of pH can be explained in terms of pH_{pzc} of Ca-montmorillonite. At pH < pH_{pzc}, the surface charge is positive, and the ion exchange between Ni^{2+} and H^+/Ca^{2+} on Ca-montmorillonite surface can lead the sorption of Ni(II) on Ca-montmorillonite.[3,4] The sorption at different ionic strength can also be used to deduce that cation exchange is the main mechanism for Ni(II) sorption on Ca-montmorillonite, especially at low pH values (Fig. SI-2†). An increase in pH above pH_{pzc} shows an increase in sorption in which the surface of the adsorbent is negatively charged, thereby it is easy for the positive charged Ni(II) to be adsorbed on the negatively charged Ca-montmorillonite surface. Another reason is that the aluminol and silanol groups of montmorillonite are less protonated with increasing pH. Hence, these groups are more available to retain Ni(II) ions. While at pH up to 10.0, the precipitation of Ni(II) may contribute to the sorption, and the precipitation have been confirmed in the following EXAFS study. In general, the effect of pH on the sorption of Ni(II) on Ca-montmorillonite is the result of the combination of the mentioned factors above. It is also necessary to note that the sorption edges spread over three pH units is often relevant of presence of many surface complexes.[3]

It can be seen from Fig. 2(A)–(C) that the sorption increases with increasing temperature in the whole pH range. The increase reflects that sorption of Ni(II) on Ca-montmorillonite is an endothermic process. Due to the endothermic ion-exchange reactions of Ni(II) ion with Ca-montmorillonite, it is reasonable that the sorption of Ni(II) increases with increasing temperature at low pH. The state and speciation of Ca-montmorillonite can also be modified with increasing temperature, which makes the direct comparison of the temperature effects for the same pH value a little difficult.[24] Tertre *et al.*[25] studied the sorption of Ni(II) on Ca-montmorillonite and found that the sorption was clearly pH dependent with a net increase of K_d (distribution coefficient) with increasing pH, which was consistent with the results of this study. Increasing reaction temperature promotes the sorption of Ni(II) on Ca-montmorillonite.

To evaluate the sorption ability of Ca-montmorillonite, sorption isotherms obtained at pH 6.4 are shown in Fig. 2(D). With increasing Ni(II) concentration, the sorption first increases rapidly

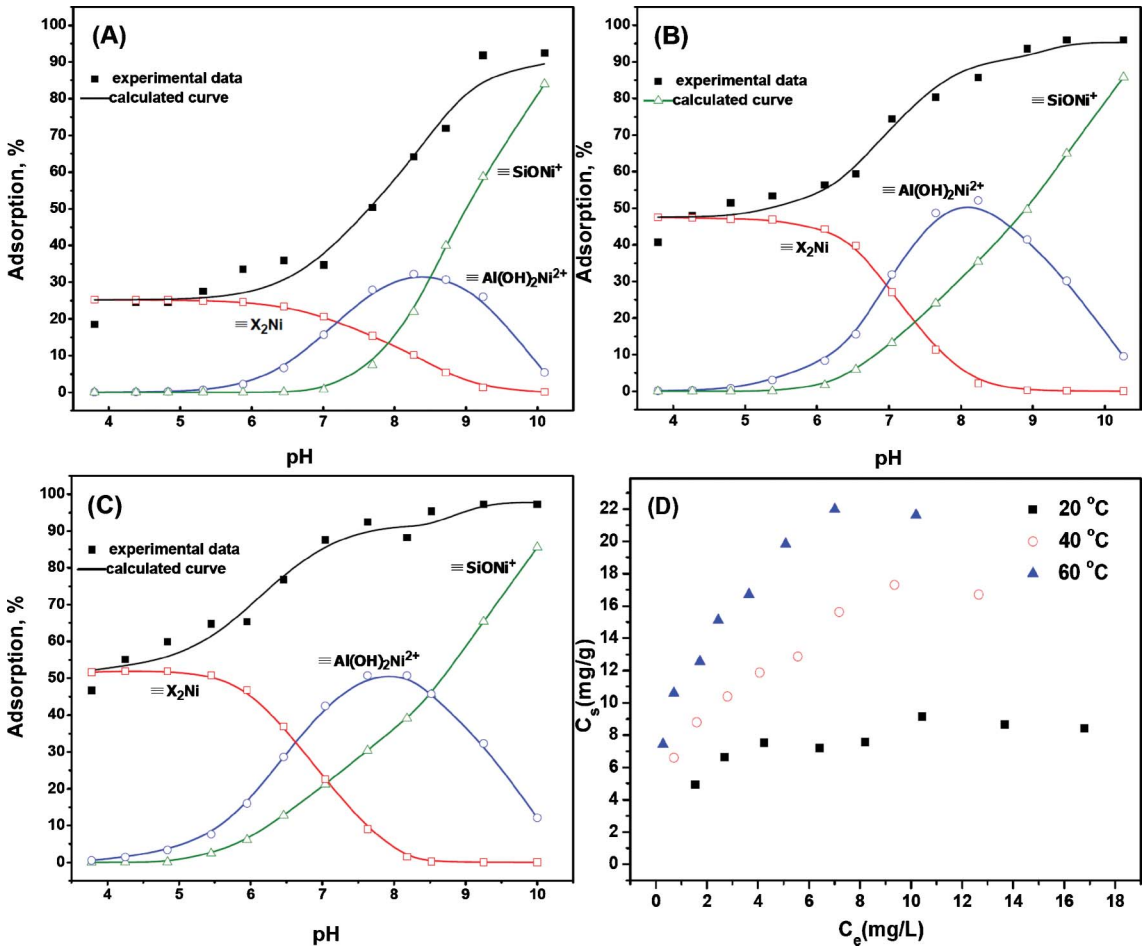

Fig. 2 Sorption percent of Ni(II) on Ca-montmorillonite and corresponding surface species repartition diagrams at temperature 20 °C (A), 40 °C (B), 60 °C (C). Sorption isotherms of Ni(II) on Ca-montmorillonite at three temperatures (D). $m/V = 0.5$ g L^{-1}, $I = 0.001$ mol L^{-1} $Ca(NO_3)_2$. (A–C): $C_{Ni(II)initial}$ = 10 mg L^{-1}; (D): pH = 6.4.

and then increases slowly. The sorption isotherm achieves the highest value at 60 °C and the lowest at 20 °C. These results indicate that high temperature favors the sorption, which agrees with the endothermic process. In order to gain a better understanding of the mechanism and to quantify the sorption data, the thermodynamic parameters (the standard enthalpy changes ΔH, the Gibbs free energy change ΔG, and the entropy change ΔS) of Ni(II) sorption on Ca-montmorillonite were determined from sorption isotherms at different temperatures. The free energy changes (ΔG) are calculated by the following equation:

$$\Delta G = -RT \ln K_{d0} \quad (4)$$

where R is the ideal gas constant (8.314 J mol^{-1} K^{-1}), T is the temperature in Kelvin, and K_{d0} is the sorption equilibrium constant. Values of $\ln K_{d0}$ are achieved by plotting $\ln K_d$ *vs.* C_e and extrapolating C_e to zero, and the value of intercept is the value of $\ln K_{d0}$. From the value of $\ln K_{d0}$, the value of ΔG can be calculated from eqn (4). The standard entropy change (ΔS) can be calculated using the following equation:

$$\Delta S = -\left(\frac{\partial \Delta G}{\partial T}\right) \quad (5)$$

Table 1 Thermodynamic data of Ni(II) sorption on Ca-montmorillonite at different temperatures

Temperature	ΔG (kJ mol^{-1})	ΔH (kJ mol^{-1})	ΔS (kJ mol^{-1} K^{-1})
20 °C	–19.54	31.81	
40 °C	–22.90	31.94	0.18
60 °C	–26.54	31.81	

The average standard enthalpy change (ΔH) is then calculated by using the values of ΔG and ΔS:

$$\Delta H = \Delta G + T\Delta S \quad (6)$$

The values obtained from eqn (4)–(6) are listed in Table 1.

As can be seen from Table 1, the standard enthalpy changes (ΔH) are positive, which indicates that Ni(II) sorption on Ca-montmorillonite is an endothermic process. Furthermore, the observed enthalpy change is greater than that for typical ion-exchange reactions (typically less than 8.4 kJ mol^{-1}),[26] suggesting that specific interactions and not only outer-sphere electrostatic interactions are operative in the Ni(II)/montmorillonite system. The Gibbs free energy change (ΔG) is negative as expected for a spontaneous process. The value of ΔG at T = 60 °C is more negative than those at T = 20 °C and 40 °C, which indicates

the more efficient sorption at higher temperature. Cations are readily desolvated at higher temperature and hence their sorption becomes more favorable. The positive values of entropy change (ΔS) reflects the affinity of Ca-montmorillonite toward Ni(II) in aqueous solutions and suggesting structure changes in the adsorbents.[27] A positive entropy change for Ni(II) sorption on Ca-montmorillonite is due to the fixation of ions on the exchange sites of the randomly distributed species on solid surfaces. This is consistent with the results that Ni(II) sorption at pH 6.4 is dominated by cation exchange and surface complexation.

At pH 6.4, Ni(II) presents in the form of octahedral hydrous Ni(II) ions ($[Ni(H_2O)_6]^{2+}$). In order to adsorb on solid surface, the hydration shell of Ni^{2+} is partially stripped. The dehydration process of Ni^{2+} requires energy, and the energy of dehydration exceeds the exothermicity of Ni^{2+} attaching to the surface. The removal of water molecules from ions is essentially an endothermic process, and it appears that the endothermicity of the desolvation process exceeds that of the enthalpy of sorption by a considerable extent.[27] This implies that structure changes in Ni(II) ions and Ca-montmorillonite units occur during the sorption process. As a result of sorption, the number of the water molecules surrounding Ni(II) decreases and thus the degree of the freedom of the water molecules increases.[26] The interpretation of the temperature-dependent sorption is further investigated at molecular level, such as the local atomic structures of Ni(II) adsorbed on montmorillonite, the transition between cation exchange and inner-sphere binding to edge sites, which are discussed in EXAFS analysis.

3.2 EXAFS Study

EXAFS is a technique to determine the local atomic structures including interatomic distances, coordination number, and type of near-neighbors surrounding surface-adsorbed metal ions and can be used to probe the mechanism of metal ion sorption to oxides and natural minerals at the molecular level. The energy and features of the main absorption edge are consistent with octahedrally coordinated Ni(II) ions (Fig. SI-3†).[13–17]

In the EXAFS analysis of references (Fig. 3), the $k^3\chi(k)$ spectrum of aqueous Ni^{2+} ions is dominated by the backscattering from oxygen atoms, resulting in one shell in the pseudo radial distribution functions (RDFs) and consistent with $[Ni(OH_2)_6]^{2+}$ octahedra. The solutions of $[Ni(OH_2)_6]^{2+}$ are immediately generated upon dissolution of simple Ni(II) salts in water containing non- or weakly-coordinating counter-anions.[28] Spectrum of the β-$Ni(OH)_2$(s) reference reveals backscattering from heavier (Ni) atoms, which represents a second shell in the RDFs. The two-shell fitting for β-$Ni(OH)_2$(s) reference sample results in the first coordination shell of 5.4 O atoms at the interatomic distances (R) of ~2.05 Å and the second-neighbor shell of 6.08 Ni atoms at the distances of ~3.11 Å (Table 2).

EXAFS data were collected for pH 5.0, 6.4, 7.5, 8.5 and 10.0 sorption samples. The k^3-weighted functions of sorption samples show distinct changes as pH increases from 5.0 to 10.0 (Fig. 3(A)). At low pH, the EXAFS spectral noise is more pronounced due to the low Ni loading on the solid surface. The spectra are dominated by O shell backscattering resembling the Ni^{2+}(aq), as expected based on the spectrum discussed above. As pH increases, pronounced features appear in the higher k range at k = 5 Å^{-1} and k = 8 Å^{-1}, which is consistent with the presence of heavy backscattering in the local coordination environment of adsorbed Ni(II).[29–31] These features indicate more than one ordered neighboring shells around adsorbed Ni atoms. Therefore, outer-sphere complexation is not the predominant sorption mode of Ni(II) on montmorillonite at high pH values.

The resulting RDFs are shown in Fig. 3(B). A broad first-shell O peak is observed for the low pH samples along with a small first-neighbor shell, and reasonable fits were obtained by fitting Ni–O shell. The EXAFS coordination number of the first shell (N_{Ni-O}) is about 6.0 (Table 2). The interatomic distance (2.03~2.04 Å) is

Table 2 Structure parameters derived from EXAFS analysis of reference samples and sorption samples at Ni K-edge

sample	Shell	R (Å)[a]	N[b]	σ^2 (Å^2)[c]	R_f[d]
β-$Ni(OH)_2$	Ni–O	2.05	5.4	0.0057	0.0027
	Ni–Ni	3.11	6.08	0.0080	
Ni^{2+}(aq)	Ni–O	2.04	5.76	0.0044	0.0034
pH 5.0, 20 °C	Ni–O	2.03	5.76	0.0054	0.0038
pH 6.4, 20 °C	Ni–O	2.04	6.09	0.0071	0.0029
pH 7.5, 20 °C	Ni–O	2.03	5.28	0.0049	0.0077
	Ni–Al	3.00	1.48	0.0052	
	Ni–Si1	3.10	2.14	0.0020	
	Ni–Si2	3.26	2.63	0.0050	
pH 8.5, 20 °C	Ni–O	2.04	5.16	0.0077	0.0072
	Ni–Al	3.00	2.04	0.0037	
	Ni–Si1	3.10	2.46	0.0042	
	Ni–Si2	3.26	3.29	0.0059	
pH 10.0, 20 °C	Ni–O	2.04	5.7	0.0062	0.0103
	Ni–Ni	3.07	3.72	0.0077	
	Ni–Si	3.26	4.2	0.003	
pH 6.4, 40 °C	Ni–O	2.04	6.16	0.0074	0.0028
pH 6.4, 60 °C	Ni–O	2.03	5.64	0.0058	0.0038
pH 6.4, 80 °C	Ni–O	2.03	5.81	0.0058	0.0045
	Ni–Al	3.00	1.84	0.0055	
	Ni–Si1	3.10	2.56	0.0030	
	Ni–Si2	3.26	3.02	0.0079	

[a] Interatomic distance. [b] Number of neighbor oxygens. [c] Debye–Waller factor. [d] The residual factor. β-$Ni(OH)_2$ and Ni^{2+}(aq) are named as reference samples, whereas the other samples of Ca-montmorillonite with adsorbed Ni(II) are named as sorption sample.

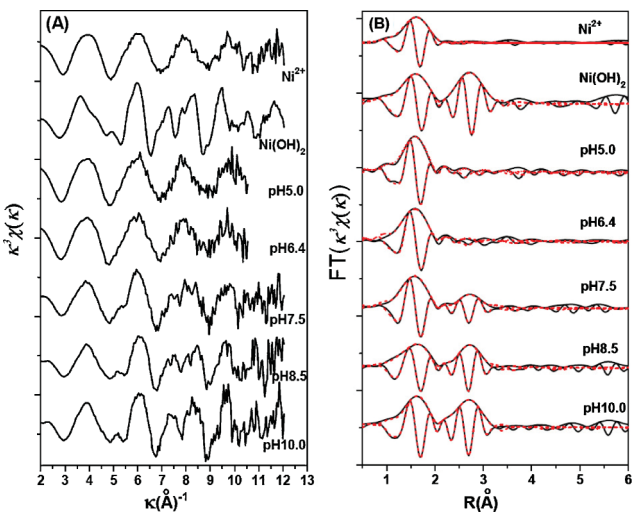

Fig. 3 Raw k^3-weighted $\chi(k)$ spectra of references and experimental samples (A) and their corresponding pseudo radial distribution functions (RDFs) (B) at different pH. m/V = 0.5 g L^{-1}, $C_{Ni(II)initial}$ = 10 mg L^{-1}, pH = 5.0, 6.4, 7.5, 8.5 and 10.0, T = 20 °C, I = 0.001 mol L^{-1} $Ca(NO_3)_2$.

typical of sixfold coordinated Ni. For all R_{Ni-O} distances fall in the 2.03~2.04 Å, we cannot explain the formation of hydrated outer-sphere surface complexes on Ca-montmorillonite as we discussed in the batch experiments. Between pH 7.5 and 10.0, a feature appearing at about 3.0–3.3 Å can be explained by the formation of surface or even polynuclear Ni complexes. The different Ni–M (M represents metal element) shell contributes to the samples prepared at high pH as determined from the fitting procedure. For the both pH 7.5 and 8.5 sorption samples, it is appropriate to fit the experimental data using a combination of Ni–Al and Ni–Si pairs, and a good fit with one Ni–Al and two Ni–Si (Ni–Si1 and Ni–Si2) pairs was obtained. Spectral analysis leads to the identification of three nearest cationic subshells containing Al at 3.00 Å, Si at 3.10 Å and 3.26 Å. The fitting data in this way gives a conclusion that inner-sphere complexes exist in our sorption samples at these conditions. These interatomic distances determined from EXAFS fitting are the characteristic of edge-sharing linkages between Al octahedra and Ni octahedral, and of corner-sharing linkages between Ni octahedra and Si tetrahedra (*i.e.*, the Ni–Si and Ni–Al interatomic distances support the formation of monodentate complexes on the Si tetrahedral and bidentate complexes on the Al octahedra), as in clay structures.[29]

At pH 10.0, the precipitation of Ni(II) may contribute to the sorption. The second RDFs peaks, however, increase in amplitude with pH increasing, but their positions remain constant. Ni(II) complexes or precipitation ($Ni(OH)_2$(s) and Ni-phyllosilicate phase) are assumed to contribute to the sorption products. In order to get accurate EXAFS fitting, the RDFs peaks in the sample at pH 10 were fitted with three models (model A: fit with O, Al, Si1 and Si2; model B: fit with O and Ni; and model C: fit with O, Ni and Si).[32–34] It can be seen from Table 3 that model A and model B have the poor fit with the reduced error $R_f > 0.02$. The samples were best fitted with ~6 Ni atoms at 3.07 Å and 4–5 Si atoms at 3.26 Å in the second coordination shell. The simultaneous appearance of the short Ni–O and Ni–Ni/Si bonds, similar to that of Ni-phyllosilicate (R_{Ni-Ni} = 3.05 to 3.08 Å, R_{Ni-Si} = 3.26 to 3.27 Å), was interpreted by the nucleation of a Ni phase having a Ni-phyllosilicate-like local atomic structure. The formation of Ni complexes or $Ni(OH)_2$(s) may not be dismissed, while we can conclude that the majority of Ni(II) sorption is through co-precipitate. The sorption product does not require the addition of Si in solution, and Si dissociate from montmorillonite facilitates the formation of Ni phyllosilicate in our montmorillonite sorption system. Dähn *et al.*[16,17] used polarized XAFS spectral analysis to distinguish whether α-Ni-hydroxide or Ni-phyllosilicate phase was formed on montmorillonite. Their results indicated the formation of Ni-phyllosilicate in the montmorillonite, which supported our results.

The effect of temperature on Ni^{2+} sorption was also selected for EXAFS measurements. The spectra of the sorption samples at pH 6.4 and the four temperature levels (20, 40, 60 and 80 °C) appear comparable (Fig. 4), but differ from either of the references, Ni^{2+}(aq) or β-$Ni(OH)_2$(s). The peak at about 2.03–2.04 Å dominates the RDFs, which has no significant difference for the four samples. EXAFS data do not suggest that the surface complexes at temperatures of 20 and 40 °C are significantly different. The second shell is not very pronounced in the RDFs except the sample prepared at 80 °C, and the heavy metal backscattering in the sample at 80 °C is more readily observed in the k^3-weighted structure. Fig. 4(A) shows the differences between the $k^3\chi(k)$ values of the samples at the four temperatures. The spectra have a beat pattern at about $k = 5$ Å^{-1} and a multifrenquence wave shape at 80 °C. These features reflect the second coordination sphere, which is indicative part of inner-sphere complexes forming on Ca-montmorillonite surfaces. EXAFS results reveal that a rise in temperature results in a gain in the inner-sphere complexation, which in turn leads to an increase in Ni(II) sorption on Ca-montmorillonite. The sorption of Ni(II) ions at the surface at elevated temperatures is likely increased due to electrostatic effects at the surface owing to a lowering of the pH_{pzc} on montmorillonite as a function of elevated temperature.[24,35] The sixfold coordination ($[Ni(H_2O)_6]^{2+}$) should also be favored entropically because of the release of H_2O to form inner-sphere complexes.[27] At pH 7.5, as can be seen from the corresponding RSFs of Ni(II) sorbed on montmorillonite for the three different temperatures (*i.e.*, 20, 40 and 60 °C) (Fig. SI-4†), the first (Ni–O) peak at R 2.03–2.04 Å remains relatively constant in amplitude with increasing temperature. The second (Ni–Al/Si) peak in the RSFs increases with increasing temperature, demonstrating the growth of the Ni(II) inner-sphere complexes with increasing temperature.

Table 3 Structure parameters derived from EXAFS analysis using different fit approach of sample at pH 10.0

Model type	Shell	R (Å)[a]	N[b]	σ^2 (Å^2)[c]	R_f[d]
Model A	Ni–O	2.03	5.4	0.0056	0.0277
	Ni–Al	3.00	2.18	0.010	
	Ni–Si1	3.10	2.24	0.0014	
	Ni–Si2	3.26	3.84	0.0040	
Model B	Ni–O	2.04	5.64	0.0060	0.0214
	Ni–Ni	3.07	5.94	0.0091	
Model C	Ni–O	2.04	5.7	0.0062	0.0103
	Ni–Ni	3.07	3.72	0.0077	
	Ni–Si	3.26	4.2	0.003	

[a] Interatomic distance. [b] Number of neighbor oxygens. [c] Debye–Waller factor. [d] The residual factor.

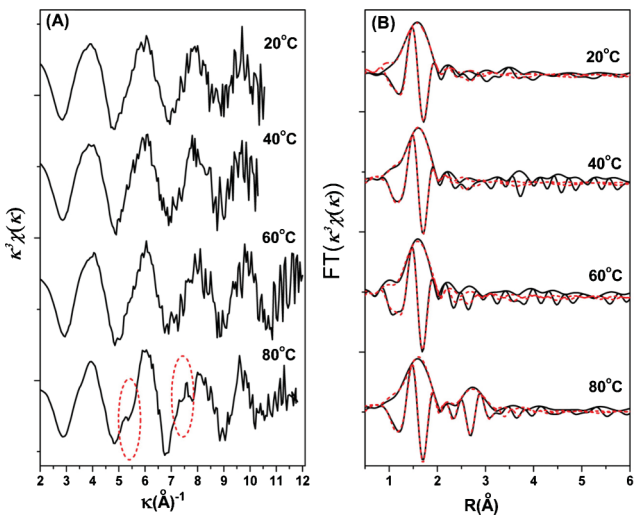

Fig. 4 Raw k^3-weighted $\chi(k)$ spectra of experimental samples (A) and their corresponding pseudo radial distribution functions (RDFs) (B) at three different temperatures. m/V = 0.5 g L^{-1}, $C_{Ni(II)initial}$ = 10 mg L^{-1}, pH = 6.4, T = 20, 40, 60 and 80 °C, I = 0.001 mol L^{-1} $Ca(NO_3)_2$.

Table 4 Surface site concentration and intrinsic surface complexation constants of Ca-montmorillonite calculated by FITEQL 3.2. C_{Solid} = 5.0 g L^{-1}, BET = 64.4 m^2 g^{-1}, N_{X2Ca} = 110 mmol/100g, I = 0.001mol L^{-1} $Ca(NO_3)_2$

	Density (mol g^{-1})				log$K$		
Site	20 °C	40 °C	60 °C	Reaction	20 °C	40 °C	60 °C
$\equiv AlOH$	1.56×10^{-4}	3.27×10^{-4}	2.69×10^{-4}	$\equiv AlOH + H^+ \Leftrightarrow \equiv AlOH^+_2$	4.40	4.57	4.65
				$\equiv AlOH \Leftrightarrow \equiv AlO^- + H^+$	−4.83	−5.59	−5.87
$\equiv SiOH$	2.43×10^{-4}	5.01×10^{-4}	5.94×10^{-4}	$\equiv SiOH \Leftrightarrow \equiv SiO^- + H^+$	−4.92	−5.12	−5.17
				$\equiv X_2Ca + 2H^+ \Leftrightarrow \equiv 2XH + Ca^{2+}$	2.46	2.51	2.53
WSOS/DF					15.12	12.19	16.02

3.3 Surface Complexation Modeling

A multisite surface complexation model was considered in this study. The sorption data modeling was completed according to the above structural investigation.

Potentiometric titrations were completed on the Ca-montmorillonite used in this study (Fig. SI-1†). The characteristics of the amphoteric behavior of the montmorillonite were described in Table 4 as well as the concentrations of each type of sites: 1.1 × 10^{-3} mol g^{-1} for exchange sites and for the edge sites, (1.56–3.27)×10^{-4} and (2.43–5.94)×10^{-4} mol g^{-1} for aluminol and silanol sites, respectively.[10,24,36]

The sorption data modeling was completed according to EXAFS structural investigation, which showed that Ni(II) was adsorbed on montmorillonite substrates as monodentate and bidentate surface complexes. The hydrolysis and aqueous complexation constants used in this work to account for nickel chemistry were those reported by Tertre *et al.*[25] We had no information regarding the number of proton released during the sorption process and the choice of the sorption equilibria were based on the goodness of the modeling for this point. The best fits were obtained considering the following sorption equilibria:

$$(\equiv X)_2Ca + Ni^{2+} \leftrightarrow (\equiv X)_2Ni + Ca^{2+} \quad (7)$$

$$\equiv Al(OH)_2 + Ni^{2+} \leftrightarrow \equiv Al(OH)_2Ni^{2+} \quad (8)$$

$$\equiv SiOH + Ni^{2+} \leftrightarrow \equiv SiONi^+ + H^+ \quad (9)$$

The surface species repartition diagrams (Fig. 2(A)–(C)) are closely linked with the EXAFS structural results, with mainly three species for pH values ranging from 3.0 to 10.0. The surface speciation diagrams show that the ion exchange species $(\equiv X)_2Ni$ is the dominant species at low pH values, $\equiv Al(OH)_2Ni^{2+}$ becomes the major species with increasing pH and $\equiv SiONi^+$ is the most abundant surface species at higher pH. The adsorbed species are same, some differences can be underlined in the surface species repartition depending mainly on pH and temperature. The global surface charge evolution of Ca-montmorillonite *versus* pH and temperature has to be taken into account to explain this behavior. The model predicts the ion exchange species $(\equiv X)_2Ni$ increase when the temperature elevate at low pH, with pH increasing, $\equiv Al(OH)_2Ni^{2+}$ and $\equiv SiONi^+$ species contribute greatly to the increased sorption as observed at macroscopic and molecular level. EXAFS shows a surface precipitate at pH up to 10.0. However, surface complexation models cannot provide an estimate of the precipitate processes, and the surface species modeling are not corresponding to the EXAFS results.

4. Conclusion

There are several different surface species that Ni(II) can be adsorbed on Ca-montmorillonite, depending on Ca-montmorillonite properties, pH, and ionic strength. At low pH, sorption is *via* ion exchange with hydrogen and calcium ions that saturate the exchange sites. Electrostatically held outer-sphere Ni(II) commonly adsorbs in the interlayers of Ca-montmorillonite. At high pH, possible inner-sphere complexes for Ni(II) sorption on Ca-montmorillonite that have been observed, which include inner-sphere surface complexes and co-precipitation. The sorption of Ni(II) on Ca-montmorillonite is the result of the combination of these factors, and the elevated temperatures lead to an increase in the inner-sphere complexation. The results are quite relevant to understand and to evaluate the physicochemical behavior of Ni(II) in the natural environment.

In the broader context of predicting Ni(II) ion mobility, bioavailability, and transport in different aqueous geochemical environments, improvements in geochemical models await further studies establishing the structural basis for Ni(II) ion sorption. The findings in this study are an important step toward a molecular-level description of Ni(II) uptake onto minerals and will help to improve our understanding of Ni(II) ion sorption processes at the water-mineral interface. More work is needed to address sorption reversibility as a function of coverage, pH and aging time *etc.* before such generalizations, if any, can or should be made in future.

Acknowledgements

Financial support from National Natural Science Foundation of China (20907055; 20971126) and 973 projects (2007CB936602; 2011CB933700) from MOST of China and Anhui Province Technology Fund for Outstanding Youths (10040606Y34) are acknowledged. The authors gratefully acknowledge Dr Bo He and Dr Zhi Xie of NSRL, USTC for helpful technical assistance of EXAFS experiments. We also express our thanks to Prof. B. Grambow (SUBATECH Laboratory, France) for favorable discussions.

References

1 R. Mandal, N. M. Hassan, J. Murimboh, C. Chakrabarti and M. H. Back, *Environ. Sci. Technol.*, 2002, **36**, 1477–1484.
2 M. Karvelas, A. Katsoyiannis and C. Samara, *Chemosphere*, 2003, **53**, 1201–1210.

3 P. Chang, X. Wang, S. Yu and W. Wu, *Colloids Surf., A*, 2007, **302**, 75–81.
4 X. L. Tan, J. Hu, X. Zhou, S. M. Yu and X. K. Wang, *Radiochim. Acta*, 2008, **96**, 487–495.
5 C. O. Ijagemi, M. H. Baek and D. S. Kim, *J. Hazard. Mater.*, 2009, **166**, 538–546.
6 S. S. Gupta and K. G. Bhattacharyya, *J. Colloid Interface Sci.*, 2006, **295**, 21–32.
7 M. E. Argun, *J. Hazard. Mater.*, 2008, **150**, 587–595.
8 K. G. Bhattacharyya and S. S. Gupta, *Adv. Colloid Interface Sci.*, 2008, **140**, 114–131.
9 M. H. Bradbury and B. Baeyens, *Geochim. Cosmochim. Acta*, 2009, **73**, 990–1003.
10 H. Marcussen, P. E. Holm, B. Strobel and H. C. B. Hansen, *Environ. Sci. Technol.*, 2009, **43**, 1122–1127.
11 M. H. Bradbury and B. Baeyens, *Geochim. Cosmochim. Acta*, 1999, **63**, 325–336.
12 B. Baeyens and M. H. Bradbury, *J. Contam. Hydrol.*, 1997, **27**, 199–222.
13 A. Voegelin and R. Kretzschmar, *Environ. Sci. Technol.*, 2005, **39**, 5311–5318.
14 A. M. Scheideger, G. M. Lamble and D. L. Spark, *Environ. Sci. Technol.*, 1996, **30**, 548–554.
15 L. Charlet and A. Manceau, *Geochim. Cosmochim. Acta*, 1994, **58**, 2577–2582.
16 R. Dähn, A. Scheidegger, A. Manceau, M. Schlegel, B. Baeyens and M. H. Bradbury, *J. Synchrotron Radiat.*, 2001, **8**, 533–535.
17 R. Dähn, A. M. Scheidegger, A. Manceau, M. L. Schlegel, B. Baeyens, M. H. Bradbury and M. Morales, *Geochim. Cosmochim. Acta*, 2002, **66**, 2335–2347.
18 C. L. Peacock and D. M. Sherman, *Geochim. Cosmochim. Acta*, 2004, **68**, 2623–2637.
19 E. Ferrange, C. Tournassat, E. Rinnert and B. Lanson, *Geochim. Cosmochim. Acta*, 2005, **69**, 2797–2812.
20 B. Ravel and M. Newville, *J. Synchrotron Radiat.*, 2005, **12**, 537–541.
21 M. Newville, P. Līviņš, Y. Yacoby, J. J. Rehr and E. A. Stern, *Phys. Rev. B: Condens. Matter*, 1993, **47**, 14126–14131.
22 A. L. Ankudinov and J. J. Rehr, *Phys. Rev. B: Condens. Matter*, 1997, **56**, 1712–1715.
23 B. Perdikatsis and H. Burzlaff, *Z. Kristallogr.*, 1981, **156**, 177–186.
24 E. Tertre, S. Castet, Z. G. Berger, M. Loubet and E. Giffaut, *Geochim. Cosmochim. Acta*, 2006, **70**, 4579–4599.
25 E. Tertre, G. Berger, S. Castet, M. Loubet and E. Giffaut, *Geochim. Cosmochim. Acta*, 2005, **21**, 4937–4948.
26 W. Li, G. Pan, M. Zhang, D. Zhao, Y. Yang, H. Chen and G. He, *J. Colloid Interface Sci.*, 2008, **319**, 385–391.
27 Q. Fan, D. Shao, Y. Lu, W. Wu and X. Wang, *Chem. Eng. J.*, 2009, **150**, 188–195.
28 Y. Xu, L. Axe, T. Boonfueng, T. A. Tyson, P. Trivedi and K. Pandya, *J. Colloid Interface Sci.*, 2007, **314**, 10–17.
29 R. Dähn, A. M. Scheidegger, A. Manceau, M. L. Schlegel, B. Baeyens, M. H. Bradbury and D. Chateigner, *Geochim. Cosmochim. Acta*, 2003, **67**, 1–15.
30 A. M. Scheidegger, E. Wieland, A. C. Scheinost, R. Dähn and P. Spieler, *Environ. Sci. Technol.*, 2000, **34**, 4545–4548.
31 D. R. Roberts, A. Scheidegger and D. Sparks, *Environ. Sci. Technol.*, 1999, **33**, 3749–3754.
32 K. Fahmy, M. Merroun, K. Pollmann, J. Raff, O. Savchuk, C. Hennig and Selenska-Pobell, *Biophys. J.*, 2006, **91**, 996–1007.
33 M. L. Merroun, J. Raff, A. Rossberg, C. Hennig, T. Reich and S. Selenska-Pobell, *Appl. Environ. Microbiol.*, 2005, **71**, 5532–5543.
34 B. K. Teo, *EXAFS: basic principles and data analysis*, Springer-Verlag Press, 1996.
35 M. Rozalén, P. Brady and F. J. Huertas, *J. Colloid Interface Sci.*, 2009, **333**, 474–484.
36 A. Kowal-Fouchard, R. Drot, E. Simoni and J. J. Ehrhardt, *Environ. Sci. Technol.*, 2004, **38**, 1399–1407.